POLITECNICO DI TORINO
Repository ISTITUZIONALE

Experimental investigation of wave-to-force modelling uncertainty for wave energy converters

Original
Experimental investigation of wave-to-force modelling uncertainty for wave energy converters / Celesti, M.L., Papini, G., Pasta, E., Peña-Sanchez, Y., Mosquera, F.D., Ferri, F., Faedo, N.. - In: MECHANICAL SYSTEMS AND SIGNAL PROCESSING. - ISSN 0888-3270. - 226:(2025), pp. 1-15. [10.1016/j.ymssp.2025.112323]

Availability:
This version is available at: 11583/2996568 since: 2025-07-24T08:47:51Z

Publisher:
Elsevier

Published
DOI:10.1016/j.ymssp.2025.112323

Terms of use:

This article is made available under terms and conditions as specified in the corresponding bibliographic description in the repository

Publisher copyright

(Article begins on next page)

27 November 2026

Mechanical Systems and Signal Processing 226 (2025) 112323

Contents lists available at ScienceDirect

Mechanical Systems and Signal Processing

journal homepage: www.elsevier.com/locate/ymssp

Invited for the special issue in honor of Professor John Mottershead

Experimental investigation of wave-to-force modelling uncertainty for wave energy converters

Maria Luisa Celesti [a,*], Guglielmo Papini [a], Edoardo Pasta [a], Yerai Peña-Sanchez [b], Facundo D. Mosquera [c], Francesco Ferri [d], Nicolás Faedo [a]

[a] Marine Offshore Renewable Energy Lab., Department of Mechanical and Aerospace Engineering, Politecnico di Torino, 10129 Torino, Italy
[b] Department of Fluid Mechanics, Mondragon University, Mondragón, Basque Country, Spain
[c] Instituto LEICI, Facultad de Ingeniería/UNLP - CONICET, Buenos Aires, Argentina
[d] Department of the Built Environment, Aalborg University, Aalborg, Denmark

ARTICLE INFO

Communicated by J. JC

Keywords:
Wave energy conversion
Experimental uncertainty
Performance assessment
Dynamical modelling
Energy

ABSTRACT

Achieving an accurate yet analytically and computationally simple mathematical model to describe the dynamical behaviour of wave energy converters (WECs) in realistic (experimental) conditions, is fundamental for optimising their performance, in particular via suitable control design procedures. Within the literature, these models are virtually always obtained by leveraging a set of simplifying assumptions on the WEC system, based on small motion about a natural equilibrium position, which does not reflect a realistic behaviour under operating controlled conditions, inevitably introducing uncertainty in the overall representation. Motivated by such an issue, this paper aims to enhance the current understanding of so-called wave-to-force WEC dynamics and to address a proper quantification of the uncertainty associated with adopting small motion assumptions in a generic form. The proposed experimental framework includes definition of the necessary tests to characterise any given WEC prototype, synthesis of representative mathematical models from the data collected, quantification and modelling of dynamical uncertainty, and consequent robust performance assessment, able to provide robust estimates of the capabilities of any (developed/novel) WEC concept at prototype stage. The methodology is illustrated by means of an experimental case study, with a small-scale prototype of the Wavestar system. Overall, the proposed framework provides valuable insights for improving WEC performance, efficiency, and reliability in practical applications, supporting decision making at early stages.

1. Introduction

In an era characterised by a growing global population, escalating energy demands, and an urgent need to address the environmental impacts of conventional energy sources, exploration of sustainable and renewable alternatives has become a fundamental concern. Among the diverse resources available, harnessing ocean wave energy stands out as a promising alternative in the pursuit of clean and efficient power generation [1]. Wave energy, due to its predictable nature and high energy density, is an ideal candidate for the renewable energy mix expansion. Overall, oceans present an untapped energy potential, that can play a crucial role in mitigating the challenges posed by climate change and resource depletion [2]. Therefore, to exploit this potential, a

* Corresponding author.
E-mail address: marialuisa.celesti@polito.it (M.L. Celesti).

https://doi.org/10.1016/j.ymssp.2025.112323
Received 5 November 2024; Received in revised form 23 December 2024; Accepted 4 January 2025
Available online 13 January 2025
0888-3270/© 2025 The Authors. Published by Elsevier Ltd. This is an open access article under the CC BY-NC-ND license (http://creativecommons.org/licenses/by-nc-nd/4.0/).

plethora of wave energy converters (WECs), *i.e.* devices capable of harnessing wave energy, have been proposed throughout recent years [3].

The need for efficient exploitation of this resource has led researchers to the development of tailored optimisation strategies. In particular, this has generated a thrust of growing focus on accurate modelling of WECs, and subsequent design and synthesis of adequate control strategies to enhance performance [4]. In fact, dynamical models fulfil a key role in effectively capturing wave energy: precise mathematical models are vital for comprehending the functionality and predicting the behaviour of WECs, enabling cost-effective design and operation, directly influencing conversion performance.

In the field of wave energy conversion, standard modelling procedures typically involve adopting a set of restrictive assumptions, in an attempt to reduce the analytical and computational complexity associated with the resulting structures. In particular, small motion assumptions (so-called linear potential flow theory) are virtually always employed to derive linear time-invariant representations for WECs, which are suitable for tractable device optimisation and real-time control design procedures. As a matter of fact, the vast majority of simulation and analysis models rely on so-called boundary element methods (BEMs), which provide a non-parametric frequency-domain characterisation of the linear behaviour of these devices about their natural equilibrium position. These linear representations, as opposed to their nonlinear counterparts, are essentially chosen due to their analytical and computational simplicity, enjoying the principle of superposition. This opens the possibility of using a vast and well-established set of tools arising from linear systems theory. Although BEM models have proven to be valuable, their validity is inherently limited to a neighbourhood of this equilibrium condition. Nonetheless, especially when under energy-maximising control, WECs motion is enhanced by the controller itself in the process of maximising performance, hence automatically deviating from the adopted linearity assumptions. In other words, the control objective pursued by WECs, *i.e.* energy maximisation, is usually obtained by enlarging the WEC operational space, contrasting directly with the small motion assumption adopted for the derivation of linear models [5]. In particular, a large amplitude motion, can drastically change the instantaneous wetted surface associated with the device, triggering nonlinear phenomena associated with the so-called *wave-to-force* representation of the WEC system (*i.e.* the map between the free-surface elevation and the force applied to the system due to the incoming wave field), by virtue of nonlinear Froude–Krylov effects. Hence, in these conditions, the validity of linear potential flow theory is no longer assured [6,7], compromising the fidelity and representativeness of the overall wave-to-motion dynamics.

Disregarding these nonlinear effects, enhanced by the controller itself, can produce wave-to-motion models with a potentially high degree of uncertainty, having a direct impact in WEC power production, with drastic performance scenarios [8]. As such, uncertainty estimation at the wave-to-force level is absolutely crucial. Regardless of the inherent characteristics and the nature of the uncertainty, it is fundamental to quantify this appropriately, allowing for its consideration within the overall control design procedure and subsequent performance assessment, and thus directly enhancing the overall WEC energy capturing capabilities and current key performance indicators for advancing wave energy conversion technology. This is particularly relevant at lower Technology Readiness Levels (TRLs), in which the decision to go from small-scale prototype to larger/full-scale development is based on performance estimation leveraging a combination of (nominal) numerical models and a limited set of experimentally tested conditions. While assessment and quantification of uncertainty have been previously performed in the literature, see *e.g.* [9–11], these studies focus on force-to-motion dynamics only, instead of addressing the uncertainty at the wave-to-force stage, being the latter predominant given the potentially large variation in the instantaneous wetted surface under controlled conditions.

Driven by the necessity of realistic assessment of the effect that wave-to-force modelling uncertainty can generate within the optimisation of wave energy conversion technology (particularly at early development stages), and its corresponding quantification in experimental scenarios, this study provides the following main contributions:

(1) Determination of an experimental procedure capable of producing representative input/output data for uncertainty quantification corresponding with the wave-to-force map for WEC systems in operating conditions. Such a procedure is based on measuring wave-generated force/torque at the specific degrees-of-freedom (DoF) to be modelled, and can be hence directly applied to any prototype WEC system.

(2) Wave-to-motion dynamical modelling based on real data, produced via the proposed experimental setup (1), and subsequent model assessment in realistic sea-state operations, elucidating the significant impact that the variation of wetted surface can have in the overall modelling procedure for WEC systems. The proposed modelling procedure is based on describing the WEC dynamics experimentally at different wetted surface conditions, leveraging input/output data in a black-box modelling framework, and can be applied to any prototype system.

(3) Generation of a family of wave-to-force models, via explicit quantification of modelling uncertainty using a frequency-domain description, employing the totality of the experimental tests available via (1) and the corresponding models derived via (2). The generated family of models is based on robust control fundamentals, in which the dynamical model identified as per our contribution (2) is used directly to find a parametric map able to describe all possible models consistent with the experimental data recorded, and be hence applied to any specific WEC concept under testing.

(4) Statistically consistent performance evaluation in terms of energy absorption and resulting operational space for realistic and experimentally generated wave conditions, leveraging the family of models defined in (3). The methodology proposed is not based on any specific assumption regarding the conversion principle, but rather on the family of models associated with the experimental data, and the sea-state conditions in which the performance is to be evaluated by the designer.

Our contributions, which aim to provide robust performance measures to support a safe transition from small-scale prototyping to full-scale developing, are demonstrated explicitly (and experimentally) by leveraging a prototype device, the so-called Wavestar system, developed and tested within the experimental facilities available at Aalborg University, Denmark. This study represents,

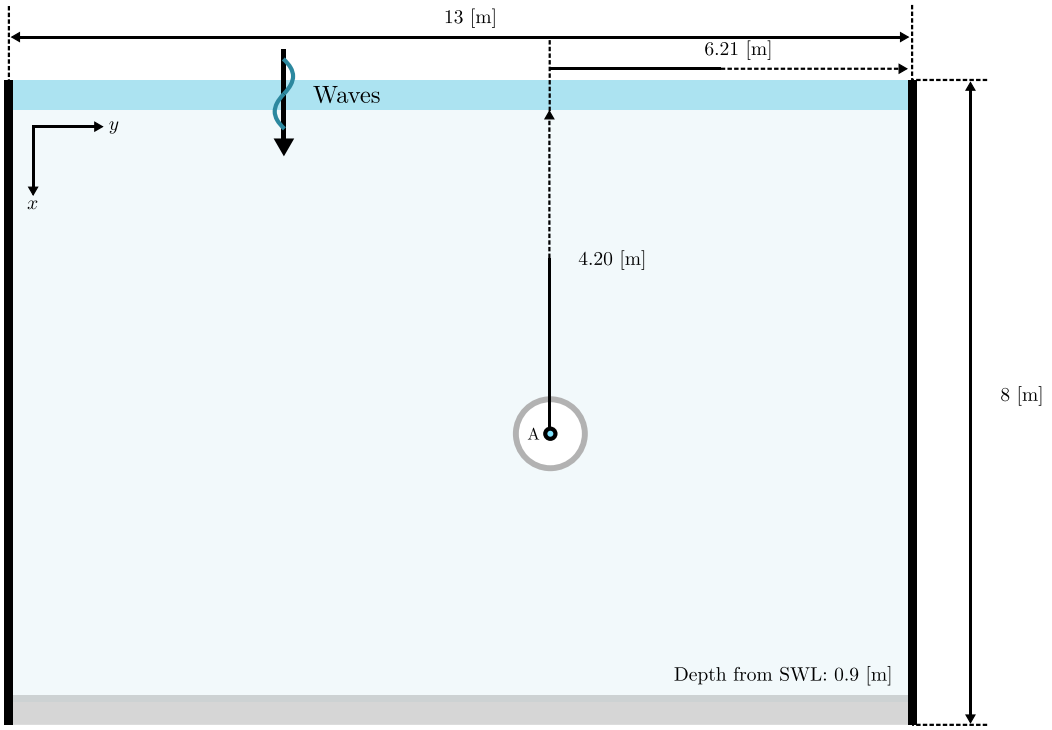

Fig. 1. Schematic illustration of the wave tank facility at Aalborg University.

to the best of our knowledge, the first experimental detailed analysis of wave-to-force modelling in accordance to the operating conditions, and its associated uncertainty, for WEC systems.

The remainder of this paper is organised as follows. Section 2 describes the experimental set-up and the facilities and prototype used within this study. Section 3 details the proposed representative input/output tests required for the proposed assessment and quantification framework, and the procedure to determine, respectively, the main device wave-to-force dynamics. Section 4 presents a detailed assessment of the computed models, highlighting the impact of different wetted surfaces in the evaluation of model fidelity, while Section 5 provides an explicit computation of the associated modelling uncertainty, and a corresponding family of WEC models for the prototype considered, including an exhaustive and consistent numerical appraisal of the performance evaluation under uncertain conditions. Finally, in Section 6, the key outcomes of this paper are summarised.

2. Prototype and experimental setup

This section provides an overview of the prototype system considered, and the testing facilities in which the experiments are conducted. Simultaneously, the experimental set-up, proposed and employed within this study, is detailed, offering the first insights into the methodological framework.

2.1. Wave tank specifications

The experimental tests are performed in the facilities of Aalborg University, in Denmark. The wave basin, represented in Fig. 1, has the following main dimensions: 19.3 [m] (length) and 14.6 [m] (width), with 1.5 [m] depth, which gives an active testing area of 13 [m] (length) times 8 [m] (width) with a fixed depth from the still water level (SWL) of 0.9 [m].

The sea states considered are generated by an actively controlled wavemaker, composed of piston-type flaps, located at the upper part of the basin (see Fig. 1), following second-order wave theory to produce long-crested waves, *i.e.* waves propagated from a single direction (in this case parallel to the y-axis and with a direction of 0°on the x-axis). In particular, the wavemaker is composed of 30 wave paddles acting in unison. Furthermore, active wave absorption is activated and implemented, to minimise the effect of reflected waves. During the tests, the prototype device is located approximately at the mid-point (both in terms of length and width) of the basin, as it can be appreciated in Fig. 1.

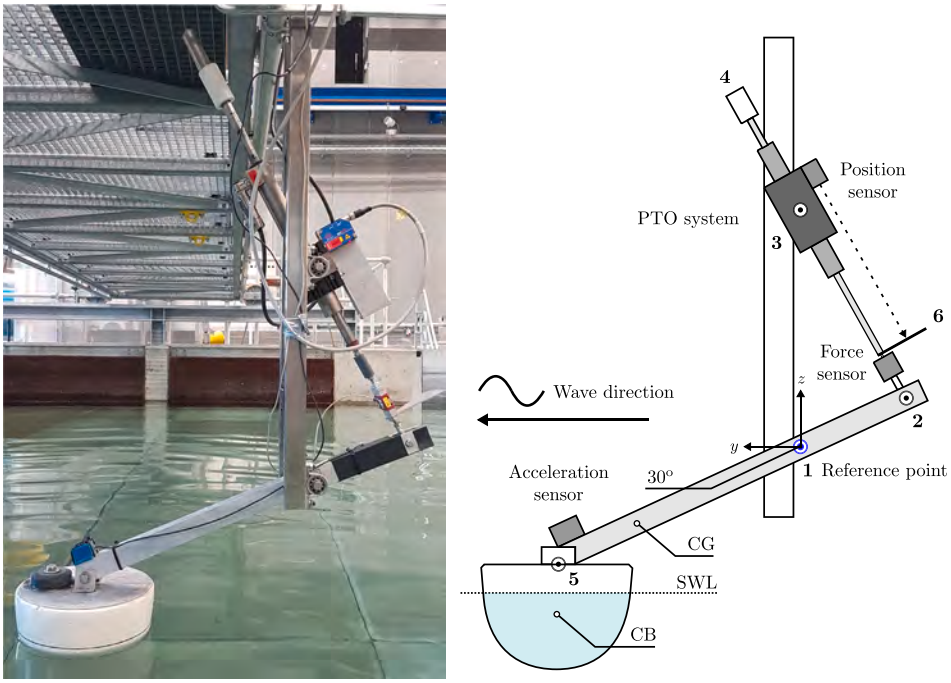

Fig. 2. Photo and schematic representation of the prototype device considered within this study.

2.2. Prototype description

The prototype device considered is a 1:20th scale of the Wavestar WEC system [12] designed within Aalborg University itself. Note that the choice of this system is motivated by the fact that this specific prototype has been chosen as a benchmark case study in well-established WEC modelling, control, and performance assessment-related research (see *e.g.* [13–16]), and hence a large pool of publicly available and transparent data can be readily found on this system, being an ideal experimental standard. The prototype WEC system consists of a wave-activated semi-sphere, with a linear electrical motor acting as a power take-off (PTO) system. The device rotates about a hinge at point **1** (see Fig. 2), and is free to move in a single degree-of-freedom, *i.e.* pitch motion about the corresponding reference point **1**. The system is equipped with instrumentation capable of measuring both linear and rotational motion, alongside the total force applied to the PTO axis, used to provide a measure for the corresponding wave excitation signals (see Section 2.3) in the adequate test conditions. Further details can be found in *e.g.* [17].

2.3. Behaviour of interest: wave-to-force dynamics

Optimising and evaluating the performance of any given WEC system normally requires two standard input/output representations: the so-called *wave-to-force* and *force-to-motion* models (see *e.g.* [18]) which, combined, ultimately generate the *wave-to-motion* behaviour of the device. These two 'stages' can be appreciated in the schematic block of Fig. 3, with specific reference to the prototype being tested (note that the schematic is, although, universal, and applies to any WEC concept, see for instance [19]). In particular, the mapping G (left) is used to denote the wave-to-force model, with h being the free-surface elevation at any desired position, p the device motion (rotational displacement) defined with respect to the reference point 1 in Fig. 2, and f_e being the resulting excitation force. Note that, in this study, the force direction is in a one-to-one relation with the DoF being modelled which, for the particular case study under scrutiny, is constrained mechanically in a single mode of motion (heave). The mapping K, instead, represents the force-to-motion response, with v the corresponding device velocity. We further remind the reader that the presented modelling architecture does not only apply to the prototype system selected, but is effectively generic, and applies to a large pool of WEC systems (see the arguments in *e.g.* [4]).

As schematised within Fig. 3 (left), the output of the mapping G, *i.e.* the wave-to-force behaviour in operating conditions (which is the core subject of our study), intrinsically depends on the actual position of the device at each time instant. This is because the total applied force from the incoming wave depends on the pressure field exerted on the device's instantaneous wetted surface, which naturally changes with WEC displacement (note that this is always the case, regardless of the WEC prototype/concept under scrutiny). Within the realm of linear potential flow theory, *i.e.* the set of assumptions virtually always adopted to derive analytically and computationally efficient WEC representations (see the discussion in Section 1), the dependence on device displacement is dropped when characterising G (as schematised within Fig. 3 - right), by assuming that the wetted surface is constant about the

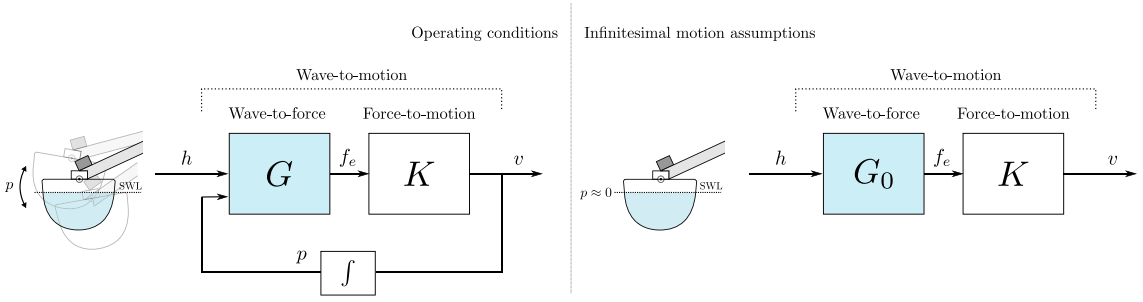

Fig. 3. Schematic representation of a WEC system in operating (left) and small motion (right) conditions.

equilibrium position, according to the SWL line. Nonetheless, when the device is under energy-maximising control in operating conditions, which often leads to large relative motions between the free-surface elevation and the device motion, the wetted surface can change considerably over time and, accordingly, there is a significant variation of the force exerted by the incoming wave field. Therefore, a simple linear model G_0, derived at the device's natural equilibrium position, independently on the instantaneous wetted surface, may no longer provide an accurate representation of the wave-to-force dynamics, deteriorating the overall wave-to-motion response. While the use of nonlinear models can offer a potential alternative and various techniques have been presented (see [18,20]), these are naturally more complex from both analytical and computational perspectives, which motivates the investigation of alternative methods to incorporate deviations from a linear (nominal) model. Within this study, the wave-to-force mapping is identified considering different (fixed) equilibrium positions, and hence different constant wetted surfaces, as further discussed in Section 3.

Regarding the force-to-motion map K, given the availability of a flexible user-defined input (*i.e.* the PTO force/torque - see *e.g.* [14,17]), computing a representative linear model can be performed more straightforwardly, leveraging standard input–output tests from the system identification and control communities. This has been performed in multiple studies featuring different WEC concepts, see *e.g.* [21–24]. As a matter of fact, for the specific prototype device considered within this paper, an open-access validated linear state-space model is readily available in [25,26], which we adopt from now on as our force-to-motion representation.

3. Wave-to-force model determination

Recall that the core objective of the study is the identification of the wave-to-force model G, as schematically presented in Fig. 3 with specific application to the considered experimental prototype device. This is performed leveraging black-box system identification techniques (see [27]), and a specific set of tests. In particular, both non-parametric and parametric models are derived based on input/output data obtained through experimental measurements taken from the system under study, in a set of tailored test conditions, as detailed within this section, aiming at circumventing the typical shortcomings from standard linear potential flow theory.

3.1. Test design and definitions

As detailed within Section 2.3, models based on standard linear potential flow theory assume a constant wetted surface, in line with the adoption of small motion assumptions (see also Fig. 3 - right). While this is effectively convenient from both simulation and control design perspectives, the map G is interconnected in a feedback fashion, *i.e.* it depends on the WEC motion itself, as can be directly appreciated from Fig. 3 (left). Aiming at retaining the convenient decoupling of the wave-to-force map G as per the linear potential flow framework, which allows for an independent design of control solutions based on the map K alone (see [4]), a generic methodology is proposed and experimentally tested within this section for the Wavestar prototype described in Section 2, which circumvents this issue by exploiting input/output data of the WEC with different (constant) wetted surfaces.

In particular, a set of (fixed) positions $\mathcal{P} = \{p_1, \dots, p_n\}$ is chosen,[1] to 'discretise' the instantaneous wetted surface space, as schematically illustrated in Fig. 4. Experimentally, the primary mover (*i.e.* floater) needs to be fixed at each p_i position, to then compute a corresponding wave-to-force model G_i based on (well-defined) input/output data.

With specific regard to the case study, during the experimental tests, the prototype Wavestar WEC device is mechanically locked at different 'equilibrium' positions. In the initial configuration, the floater arm is tilted at an angle of 30°with respect to the SWL. Throughout the paper, this is referred to as *nominal* position/configuration, since this is the natural equilibrium of this specific prototype system, and the specific point that is commonly used to derive the nominal model G_0 in Fig. 3 (right), using linear potential flow theory assumptions. The other locking positions for the device are obtained by both increasing and decreasing the

[1] For the case of multi-float systems, the procedure requires a multiple-output representation. This, in turn, necessitates a definition for the fixed positions according to the specific concept under scrutiny, in line with the corresponding variation of the wave-to-force model.

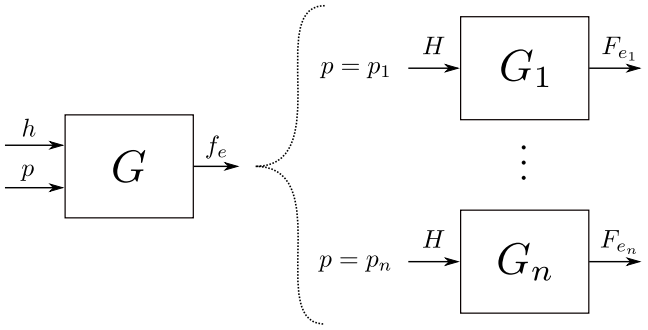

Fig. 4. Proposed 'discretisation' procedure for the computation of the wave-to-force model characterising the WEC system.

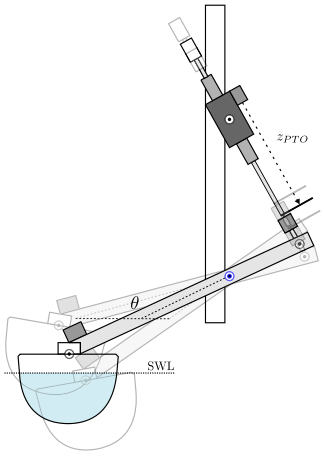

(a) Schematic illustration of the variation in position.

Position i - G_i	z_{PTO} [mm]	θ [rad]
1 - G_1	20	0.423
2 - G_2	10	0.473
0 - G_0	0	0.523
3 - G_3	-10	0.573
4 - G_4	-20	0.623

(b) Position specification for uncertainty quantification tests.

Fig. 5. Uncertainty quantification test specifications.

angle of the floater, considering variations about the nominal position. Experimentally, this angular variation can be translated to a fixed linear displacement of 10 [mm] along the z_{PTO} direction between each case, as can be seen in Fig. 5. Note that the procedure proposed is effectively WEC-agnostic, requiring only to lock the primary conversion stage (floater) at different wetted surface configurations, according to the concept being experimentally tested.

To experimentally characterise the considered WEC system, potentially operating in a broad range of conditions, banded white-noise spectra, *i.e.* with a constant spectral density function, are adopted as input signals, to identify each G_i system in Fig. 4, according to the generic prototype locking procedure described in Fig. 5. In particular, two different white noise sea states (termed WNSS1 and WNSS2, respectively, in line with [17]) with the same bandwidth (0.1 [Hz] to 2 [Hz]) and with progressively increasing energy are considered, as per Fig. 6. The choice of the frequency band, for the experimental case study presented, is performed taking into consideration the main dynamics of the prototype, and the intrinsic physical limitations of the wave tank facilities, *i.e.* the mechanical wavemaker, while the choice of increasing energy for the input signal is driven by the fact that, in this way, it is possible to appreciate the effect of higher energy content on the system response and to highlight (on average) eventual nonlinear behaviour of the WEC prototype (see *e.g.* [28]), for each fixed position p_i. This helps in reducing the variance of the empirical responses computed hereinafter.

The first test performed within the experimental campaign has the objective of providing the time series associated with the free-surface elevation h for each white-noise sea state considered, which represents the set of input signals for identification. These measures are taken without the presence of the device in the tank, using a wave probe positioned in the point indicated with A in Fig. 1, which corresponds to the centre point of the WEC. An example of these input waves arising from this test can be appreciated in Fig. 6, which illustrates the frequency content associated with each sea state (top), in terms of the corresponding discrete Fourier transform (DFT), and a snippet of the time-domain traces.

After obtaining the measurements of the free-surface elevation, the wave excitation force/torque acting on the WEC is measured, for each specific wave generated, and each fixed position p_i. This is performed with the device blocked in the desired position (as per the discretisation presented in Fig. 5(b)) within the tank. The force exerted by each wave can be then measured by the load

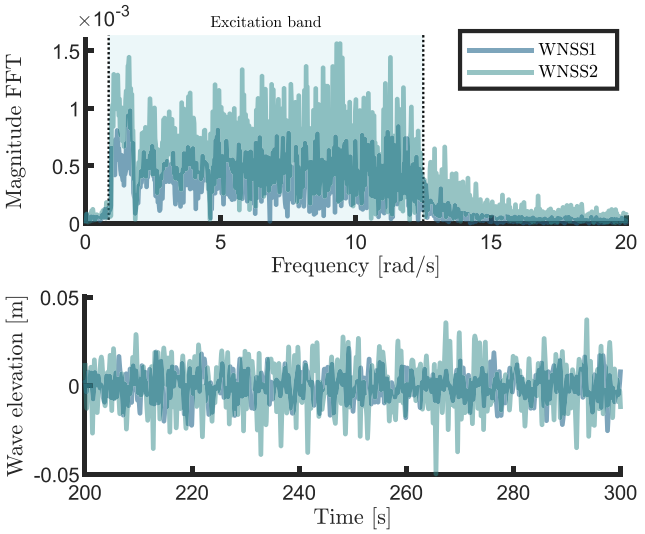

Fig. 6. White noise waves - Experimental free-surface elevation both in frequency (magnitude - top) and time (bottom).

cell connected to point 2 (see Fig. 2). These tests are systematically re-executed for each locking position taken into consideration within the study.

3.2. System identification

Having measured experimentally according to the proposed procedure, for each locking position considered, the sets of inputs (wave elevation) and outputs (excitation force) signals, it is possible to define the so-called empirical transfer function estimates (ETFEs) for each input/output pair. These estimates, and the procedure described within this section, are fully based on experimentally recorded input/output data, and hence completely generic and applicable to any prototype under testing. In particular, the applied input and recorded output can be described, respectively, through the sets $\mathscr{H} = \{h^j\}_{j\in\mathcal{I}_j}$, and $\mathscr{F} = \{f_{e_i}^j\}_{(i,j)\in\mathcal{I}_i\times\mathcal{I}_j}$, where $\mathcal{I}_i = \{0,1,2,3,4\}$ is the set containing the different locking positions considered (as per Fig. 5(a)), while the set $\mathcal{I}_j = \{1,2\}$ refers to the input sea states considered (WNSS1 and WNSS2). A non-parametric frequency-domain description of the wave-to-force mapping, $h \mapsto f_e$, hence a linear characterisation of the operator G_i for each locking position, can be computed as follows:

$$G_i^j(\jmath\omega) = \frac{H^j(\jmath\omega)}{F_{e_i}^j(\jmath\omega)}, \tag{1}$$

where capital letters indicate Fourier transform pairs. Afterwards, an average of input/output pairs, associated with different incoming sea states, is performed to produce a low variance set, computed as:

$$\bar{G}_i(\jmath\omega) = \frac{1}{\#\mathcal{I}_j}\sum_{j=1}^{\#\mathcal{I}_j}\tilde{G}_i^j(\jmath\omega). \tag{2}$$

To enhance the precision of the overall identification process, a suitable split of the input and output signals is performed. Specifically, a Bartlett-type averaging method (see [29]) is employed, followed by an average on each sea state. Given the utilisation of non-periodic signals, and to mitigate signal discontinuity arising from the periodic extension inherent in DFT computations, a moving average filter is applied to Eq. (1). The outcome of such a system identification procedure is exemplified in Fig. 7, specifically for the so-called nominal configuration case, *i.e.* G_0 (see Section 3).

Regarding the dynamical structure underlying each map G_i, note that the wave-to-force system is inherently non-causal, *i.e.* the generated wave (free-surface elevation) may impact the WEC body and exert a wave force before any wave has reached the device 'centre' [30]. This non-causality can be written analytically in terms of a time-advance τ, and hence the ETFE in (2) can be seen, without any loss of generality, as the product of two components. Specifically:

$$\bar{G}_i(\jmath\omega) = e^{\jmath\omega\tau}G_c(\jmath\omega), \tag{3}$$

where G_c is the causal component, while $e^{\jmath\omega\tau}$ is the frequency-domain representation of the corresponding time-advance. The specific value for τ is generally unknown in experimental scenarios and depends on the geometry and size of the considered device.

With the definition of the non-parametric ETFE in (2), for each specific locking position, a parametric identification is sought, to produce models useful for time-domain simulation and control design and synthesis. To achieve such a parametric form, frequency-domain subspace-based methods, as described in [31], are employed to establish a continuous-time state-space system. Nonetheless,

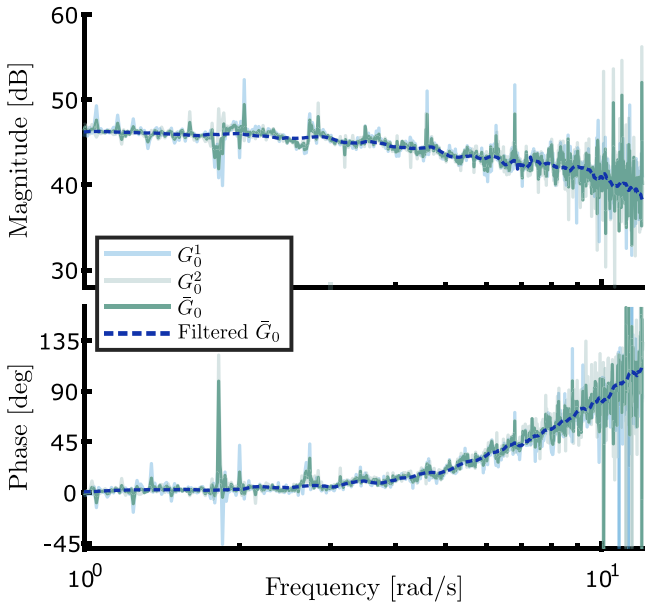

Fig. 7. Non-parametric responses for the experimental wave-to-force map in the nominal configuration condition.

a direct application of standard subspace identification for (3) is not possible without prior knowledge of the advance value τ. To address this issue, and compute both a state-space finite-dimensional approximation of G_c and an estimate for τ simultaneously, the following algorithm is employed:

- ▷ Select a trial advance set $\mathcal{T} = \{\tau_k\}_{k=1}^{P}$ and order $\bar{n}$.
- ▷ **For** $j = 1 : P$ **do**:
  - $T_c = \tau_j$
  - $G_c(j\omega) = e^{-j\omega T_c}\bar{G}_i(j\omega)$
  - $\Sigma_j = \text{identify}(G_c, \bar{n})$
  - $e_j = \|e^{j\omega T_c}\Sigma_j(j\omega) - \bar{G}_i(j\omega)\|_2^2$

  end
- ▷ Choose $G_i = \Sigma_J$, with $J = \arg\min_j\{e_j\}$.

The pseudocode above can be motivated as follows. Since the value for τ is generally unknown, the user selects a trial set of values $\mathcal{T}$. For each value in this set, the frequency response associated with the (causal) map G_c is constructed from the corresponding filtered ETFE, and a corresponding state-space approximation of order $\bar{n}$ (defined via singular value decomposition of the Hankel matrix associated with the ETFE data) is computed using subspace identification (indicated in the algorithm above with the generic function 'identify'). Finally, the system producing the lowest fitting error (in a 2-norm sense) is chosen, together with its corresponding advance value.

The full process is executed for each corresponding locking position, to derive an associated parametric representation. The final results arising from the proposed procedure are illustrated in Fig. 8. In particular, the figure presents, for each locking position, the identified parametric mapping and the associated filtered non-parametric ETFEs (transparent lines), in terms of magnitude and phase. Note that, for reference, in the same figure, a characterisation of the wave-to-force response of the prototype system in the nominal configuration, computed numerically using the BEM solver NEMOH [32], is included (dashed), for the sake of benchmarking and comparison. The latter is effectively the standard modelling procedure employed within the literature to derive a dynamical WEC model for control and performance assessment purposes. The different behaviour, manifested by each locking position, which is already evident in the Bode plot presented in Fig. 8, is further discussed in the following sections, together with its overall impact on the wave-to-motion dynamics of the WEC.

4. Model quality assessment

To assess the overall influence of the locking position, and hence the corresponding wetted surface considered (see Section 3.2), a detailed assessment is performed, according to different operating conditions. In particular, the aim is to assess the reliability and accuracy of the wave-to-force model for its intended use, and the representativeness of each G_i according to the specific sea-state

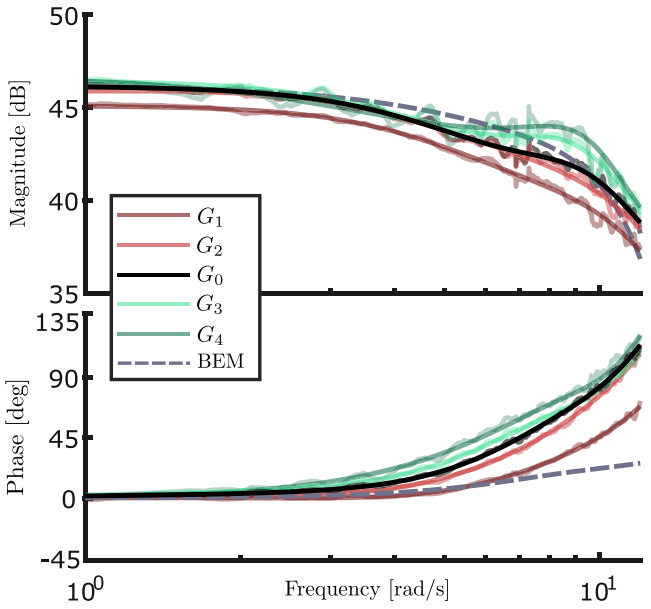

Fig. 8. Comparison of the identified wave-to-force model depending on the different positions (solid), and BEM response (dashed).

condition. The assessment process presented within this study involves the execution of multiple experiments, as further detailed in Section 4.1. Subsequently, the outcomes for the so-called nominal configuration case, and each locking position, are reported in Section 4.2. Various key parameters are considered to evaluate whether a given model, computed in a given fixed position, is more suitable for any specific sea-state condition, highlighting the influence of the adopted modelling assumptions.

In the following, an in-depth analysis of the performance and behaviour of each of the developed models G_i is presented, to gain an understanding of the role and accuracy that can be attained according to the specific operating conditions. In other words, and as explicitly shown and demonstrated within this section, the model arising from the nominal configuration (*i.e.* assuming the standard equilibrium SWL line, according to the natural equilibrium position of the WEC) - which is the largely dominant choice within the WEC modelling literature - does not necessary constitute the most accurate representation, and its performance depends on the specific sea-state condition. This is because the small motion assumptions prioritising the nominal case, no longer hold, particularly with sea states closer to the device resonance.

4.1. Test design for model assessment

Naturally, model assessment is performed considering a new set of data, not used for the system identification procedure. In particular, as opposed to banded white noise (as per the procedure performed in Section 3.2), irregular waves, which are representative of realistic operating sea-state conditions, are considered for the model assessment stage. In particular, irregular waves can be characterised in terms of a stochastic process, with an associated power density. Within this study, the JONSWAP spectrum [33] is considered, which can be fully defined by three main parameters: significant wave height, H_s, peak period, T_p, and peak-enhancement factor, γ. Three irregular sea states (SS1, SS2 and SS3) are considered for assessment within this experimental campaign, with characterising parameters reported in Table 1. As can be appreciated from their theoretical spectra reported in Fig. 9, the sea states considered aim to represent different operating conditions. While SS1 and SS2 are two narrow-banded conditions, SS3, also presenting a lower wave height, represents a broad-banded operating condition, closer to the device's resonant behaviour. For each sea state, to give a statistically consistent representation of the operating conditions, $\approx$ 200 periods are generated within the wavetank, and considered subsequently for model assessment. Overall, the chosen sea states, going from low to high frequency, cover the range of main interest for the device analysed within this study. This can be concluded directly from Fig. 9, where a characterisation of the I/O magnitude responses (wave-to-force, force-to-motion and wave-to-motion) of the prototype system, computed numerically using BEM software with the device in the nominal configuration, is included, for reference.

4.2. Numerical appraisal

This section presents a numerical appraisal of the accuracy that can be obtained with each derived model, according to the specific locking position. This is performed both in a wave-to-motion (velocity) fashion, *i.e.* from measured free-surface elevation h to overall device output velocity v.

Table 1
Parameters characterising the irregular sea states used for model assessment purposes.

Sea state	H_s [m]	T_p [s]	γ
SS1	0.063	1.412	3.3
SS2	0.104	1.836	3.3
SS3	0.021	0.988	1

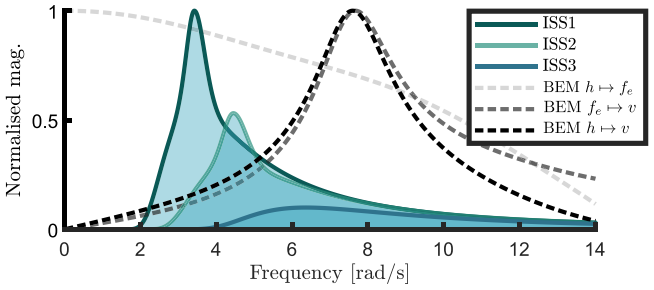

Fig. 9. Irregular waves theoretical JONSWAP spectra (normalised with respect to the maximum peak encountered, which corresponds to ISS1) used for assessment, overlap with the device theoretical BEM responses (normalised with the respect to its own maximum absolute value), for the nominal configuration.

Table 2
NMAPE corresponding to the wave-to-velocity mapping for each locking position.

Locking position i - G_i	NMAPE [%]		
	SS1	SS2	SS3
1 - G_1	10.51	7.43	9.69
2 - G_2	6.31	4.47	6.63
0 - G_0	3.72	4.30	7.64
3 - G_3	4.42	5.69	9.63
4 - G_4	4.52	3.75	6.58

To quantify the accuracy and reliability of the models, different key metrics are taken into account. In particular, in the first stage, the normalised mean absolute percentage error (NMAPE) is selected as a standard accuracy indicator (see *e.g.* [34,35]), defined as

$$\text{NMAPE}(y, y_r) = \frac{100}{N} \sum_{i=1}^{N} \frac{|y(t_i) - y_r(t_i)|}{\max(|y_r(t_i)|)}, \tag{4}$$

where N denotes the number of (time-domain) samples available for the generic time traces of the target (reference value, y_r, obtained directly from the measurement of linear acceleration (see Fig. 2)), and the output signal, y. The models are assessed by comparing their outputs (*i.e.* excitation force and device velocity) with reference values obtained, measured experimentally.

Table 2 offers an appraisal of the NMAPE value for each corresponding model G_i, with $i \in I_i$ being the specific locking position used to compute the dynamical representation, according to Section 3.2. One major conclusion can be drawn almost immediately: according to the wave condition, each derived model, in diverse (constant) wetted surface conditions, presents a different accuracy. In other words, the standard approach pursued in the literature, *i.e.* computing a single model about the natural equilibrium position - G_0 - does not necessarily produce the best outcome in terms of wave-to-motion accuracy. For instance, SS2, being a more energetic sea state, generating in this case larger overall motion, is better represented by G_4, which is derived with the device in a fixed locked position 'deeper' than its nominal configuration (see Fig. 5(b)). A similar behaviour can be appreciated for SS3 which, though less energetic, is closer to the device resonance condition, also enhancing the overall prototype motion. This suggests that an accurate wave-to-force model should be computed according to the specific objective and/or sea-state condition, which is certainly not necessarily the currently dominant approach within the literature.

To further explore the accuracy of these models, and given the major role played by a good instantaneous phase synchronisation in control design and synthesis (see *e.g.* [36]), cross-correlation and instantaneous phase error (leveraging the Hilbert transform) between measured and predicted velocity, are reported in the following. Fig. 10 presents these two key parameters, *i.e.* cross-correlation, and instantaneous phase difference, for each locking position and associated model G_i. The latter metric is shown on a polar histogram, where the instantaneous phase alignment between target and model output signals can be effectively appreciated in terms of their occurrence, whose level of a certain phase difference is indicated with the bar height oriented in the value representing the corresponding phase difference. In particular, Fig. 10 offers a comparison of cross-correlation and instantaneous phase difference across the different locking positions examined for the device, encompassing each sea state assessed during the validation.

As per the NMAPE, according to the sea state considered for the assessment, there is a different correspondence between the various locking positions and associated force-to-motion dynamics. Specifically, for SS1 (top-graph) there is an almost perfect

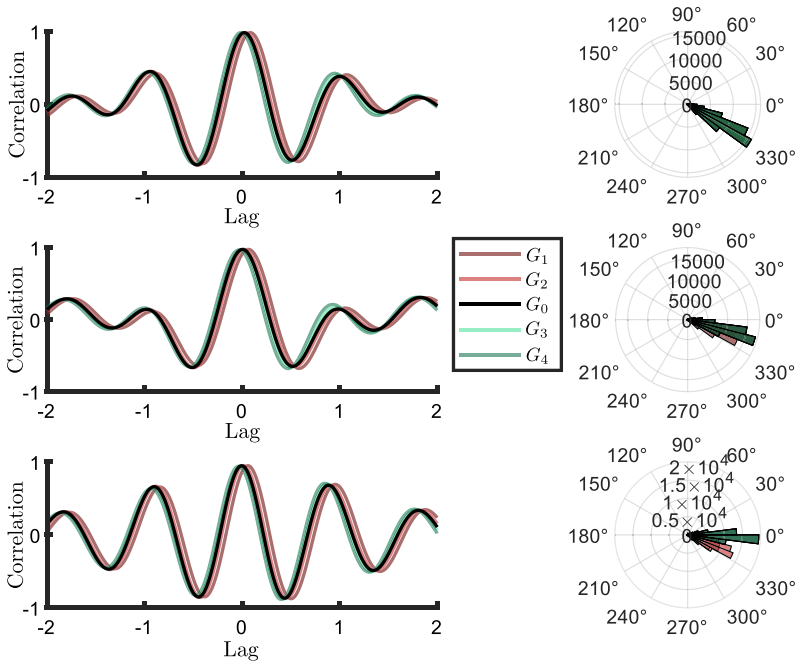

Fig. 10. Cross-correlation and instantaneous phase difference for each locking position in relation to the sea state (from top to bottom: SS1, SS2, SS3).

superposition in terms of instantaneous phase difference occurrences for the various cases considered, while the cross-correlation presents some small misalignments, with the nominal case achieving the best performance, *i.e.* reaching the maximum correlation value for a lag almost equal to zero, consistent with the NMAPE results presented in Table 2. Instead, considering SS3, models derived with the device locked in configurations (3) and (4) (see Fig. 5) present values that reflect an increased correspondence between model output and experimentally measured data. This is also consistent with the results in Table 2 and stresses that the standard modelling approach (nominal configuration) does not necessarily deliver the best results in terms of fidelity.

5. Performance assessment under uncertainty

The results presented in Sections 3 and 4 stress the fact that a single wave-to-force model, computed in the standard nominal configuration, does not tell the full story: the dynamics of the WEC can change significantly as a function of the instantaneous wetted surface, and hence both control design and synthesis, and device performance assessment (especially with the scope of WEC optimisation), need to be performed by considering the uncertainty introduced by the widely adopted small motion modelling assumptions. Motivated by this, and leveraging the experimental test design procedure proposed in Section 3, and the corresponding dynamical models (with parametric responses summarised in Fig. 8), a family of possible WEC systems is derived within this section, via quantification of the associated modelling uncertainty. Such a family is then subsequently employed to analyse the performance of the WEC prototype, in different energy-maximising control conditions, providing an assessment framework consistent with the modelling uncertainty.

In particular, a family of models $\mathcal{G}$ based on an additive structure is considered, described through an unstructured uncertainty set

$$\mathcal{D} : \{\Delta \in \mathcal{H}_\infty \mid \|\Delta\|_\infty < 1\}, \tag{5}$$

and hence the family $\mathcal{G}$ can be described in terms of (5) as

$$\mathcal{G} : \{(G, \Delta) \in \mathcal{H}_\infty \times \mathcal{D} \mid G = G_0 + W_\Delta \Delta\}, \tag{6}$$

where W_Δ is the so-called uncertainty weight, which essentially describes how uncertainty is distributed in frequency. Note that G_0, *i.e.* the dynamical model associated with the nominal configuration, has been selected in this section as the nominal model for the description of the family $\mathcal{G}$, motivated by the standard procedure adopted within the literature. We do remark that this choice can be performed by exploiting the analysis provided in Section 4, and hence adopting a (different) nominal model depending on the operating conditions. We further note that the definition of the family (6), and the experimental identification of the uncertainty weight as described below, can be performed for any WEC concept under testing, as is not limited to the Wavestar case study under scrutiny, hence being completely generic and agnostic with respect to the conversion principle.

The characterisation of the uncertainty weight W_Δ is performed in the frequency domain, based on the maximum distance between the parametric model associated with the nominal case and those related to each different locking position at that each

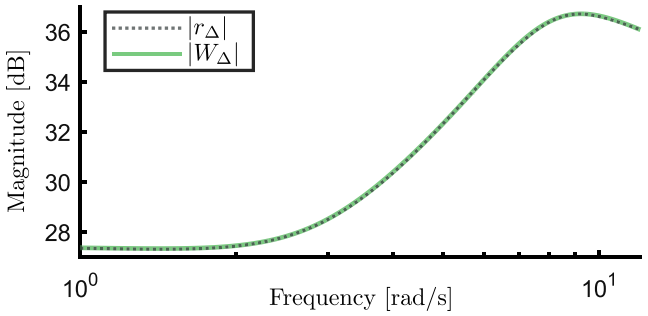

Fig. 11. Uncertainty weight definition for the WEC prototype.

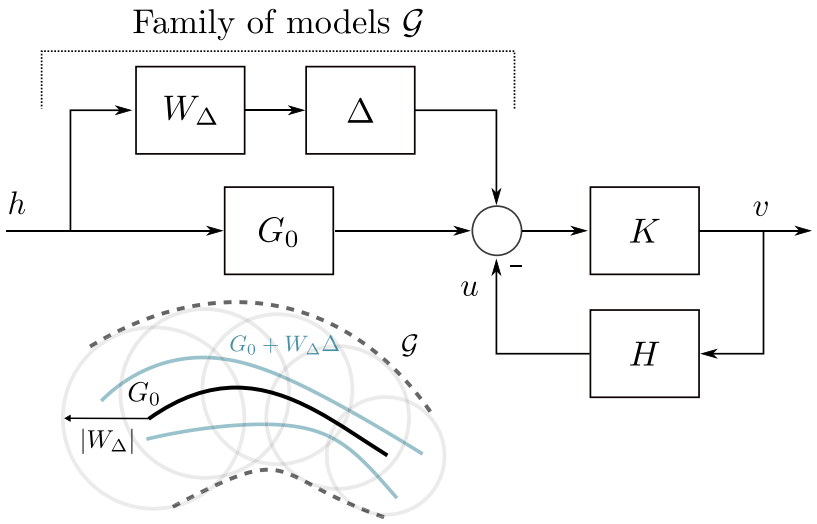

Fig. 12. Schematic diagram for the simulation loop considered for energy absorption assessment over the identified family $\mathcal{G}$.

frequency. In particular, W_Δ is computed such that the following condition

$$\left|W_\Delta(j\omega)\right| \geq r_\Delta(\omega) = \max_{j\in I_j} \left|G_i(j\omega) - G_0(j\omega)\right|, \tag{7}$$

holds, where $G_i(j\omega)$ is the parametric response corresponding to each parametric model computed, while $G_0(j\omega)$ is the frequency response associated with the nominal position. The map r_Δ in (7) describes, in essence, the smallest radius including all possible plants in $\mathcal{G}$. A parametric description for W_Δ, consistent with (7), can be computed by leveraging standard filtering realisation techniques (see *e.g.* [27]). The results for the identification of the corresponding family can be appreciated in Fig. 11. In particular, Fig. 11 shows an appraisal of the map r_Δ, and the corresponding identified weight W_Δ (order/dimension 4), fulfilling (7).

The definition of the family of systems $\mathcal{G}$, consistent with the experimental tests and data obtained in different locking conditions, allows for a statistically consistent performance assessment of the WEC prototype. In particular, to illustrate the assessment framework and overall results, 200 possible systems $G \in \mathcal{G}$ are considered, by random generation of elements in the set $\mathcal{D}$(5), and used to compute final energy absorption in all three operating conditions (SS1, SS2 and SS3). A standard PI control configuration (referred to in the literature of WEC technology as a 'reactive' controller) is utilised, where the parameters are sea-state dependent, and have been optimised to maximise energy absorption in-situ, as detailed in [17]. The overall performance assessment scheme is presented in the block diagram of Fig. 12.

The randomly selected wave-to-force models for simulation and performance assessment can be appreciated in the Nyquist diagram of Fig. 13. In particular, the response associated with the nominal model G_0 is denoted with solid circle markers, while the corresponding disk uncertainty, following equation (7), is illustrated with full circles of radius $W_\Delta(j\omega)$, centred at $G_0(j\omega)$. Inside this family, the 200 randomly generated systems for simulation and assessment are denoted with transparent blue lines, with responses naturally contained within $\mathcal{G}$, as per equation (6).

Leveraging the computed family $\mathcal{G}$, and the associated randomly generated elements (as per Fig. 13), Fig. 14 presents a histogram of the mean power absorbed for each simulated WEC case, and each of the sea states listed in Table 1, normalised by the mean power absorbed if we consider the nominal model G_0 for each specific operating condition, computed in the nominal configuration

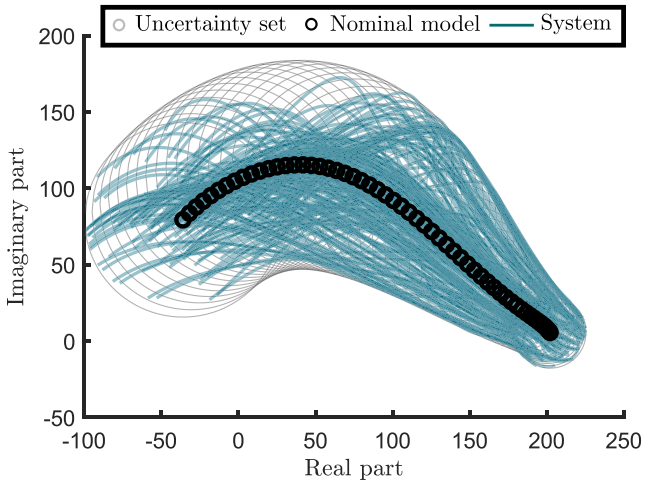

Fig. 13. Representation of the wave-to-force family of models $\mathcal{G}$ for the experimental prototype WEC system, and the corresponding 200 randomly selected candidates for assessment. Note that the uncertainty is represented with grey circles.

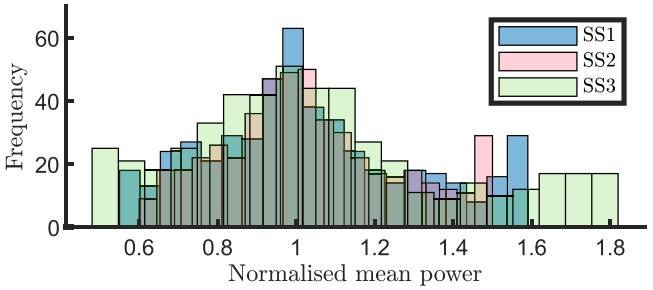

Fig. 14. Histogram of normalised mean power absorption, considering the 200 randomly generated elements in $\mathcal{G}$. Note that transparency is used to enhance presentation due to overlapping.

described in Section 3.2. At first glance, a largely spread distribution can be appreciated, with maximum variations of up to 60%–80% of the nominal expected absorption, according to the sea-state case. Note that, for the case of SS3, being broadband and with a peak frequency closer to the resonant behaviour of the system, the mean power computation for each model generated within the family tends to be more sparse than in the SS1 and SS2 cases. This is indeed consistent with the results presented in Figs. 8 and 11, *i.e.* a larger modelling uncertainty is present in a neighbourhood of the device resonant behaviour. This highlights the necessity of considering the corresponding modelling uncertainty also when assessing a WEC under energy-maximising conditions, and being able to compute a consistent measure of performance.

To conclude with the presented assessment, Fig. 15 illustrates, in sampling counts, the normalised absolute value of the WEC position, for each simulated WEC system generated within $\mathcal{G}$, and operating sea state. The normalisation is performed with respect to the maximum absolute value of displacement associated with the nominal representation G_0, for each operating condition considered. As per Fig. 15, a large variation of operational space can be appreciated, for all sea states considered. Such a variation can go to up to 20% of the maximum value estimated by considering in simulation the nominal model G_0 only, hindering potentially large motions that can be later found in practice. Once again, and consistently with what is discussed within this section, SS3 presents the largest variability, also in terms of device displacement among the generated members of the family $\mathcal{G}$. These can naturally generate fatigue excess in device components if not dimensioned accordingly a-priori, reducing its overall lifetime, and increasing maintenance requirements. This information, as well as the mean power variation presented within Fig. 14, are fundamental assets for proper device design and optimisation, being able to provide reliable statistical information on the main relevant indicators for successful WEC technology.

6. Conclusions

This paper highlights, in a fully experimental scenario, the impact of the modelling uncertainty generated by adopting small motion assumptions, to derive WEC models based on linear potential flow theory. An explicit quantification of such uncertainty is

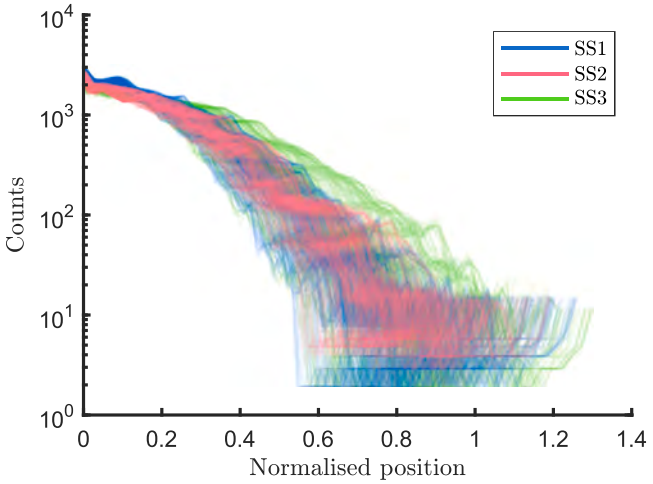

Fig. 15. Normalised absolute value of position, for each of the 200 systems generated within $\mathcal{G}$, and operating sea-states.

pursued systematically, by proposing a set of tailored experiments, aiming to circumvent the typical issues of the standard modelling route pursued in the literature. Once quantified, parametric models are derived for the WEC system in different wetted surface conditions, and leveraged to build a family of possible WEC systems described by the experimental data, generating a fundamental asset for statistically consistent performance evaluation under uncertainty. The presented procedure is entirely generic and WEC agnostic, and can be hence applied to any prototype conversion concept under testing.

In particular, considering a prototype WEC device in different (locked) positions, the wave-to-force response is characterised experimentally according to different (constant) wetted surfaces, via both non-parametric and (subsequent) parametric system identification procedures. With the derived models, the impact of the widely adopted small motion modelling assumptions is assessed systematically, by elucidating the accuracy of each representation according to the sea-state condition. It is shown that the nominal approach, which is virtually always adopted within the state-of-the-art, does not necessarily offer the best results in terms of representing the WEC behaviour, and that other (constant) wetted surface conditions can provide a more accurate prediction of the device motion.

Motivated by these results, and leveraging the same input/output dataset and derived models, the corresponding modelling uncertainty is quantified and parameterised accordingly, in terms of a family of WEC models described in terms of an unstructured additive framework. The resulting family is then used to assess the performance of the WEC prototype under controlled conditions, in diverse operational sea states, providing a statistically consistent measure of energy absorption and overall operational space. Variations of between 60%–80% can be appreciated in these key indicators with respect to the nominal case, highlighting the fundamental relevance of considering modelling uncertainty properly when assessing the potential of any given WEC system.

Overall, the procedure proposed in our paper to (1) carry out the adequate experiments to characterise a WEC prototype, (2) synthesise representative mathematical models from the data collected, (3) quantify and model the dynamical uncertainty incurred, and (4) perform a statistically consistent performance assessment, provides a robust estimation framework to test the capabilities of any (developed/novel) WEC concept at prototype stage, supporting decision making at early stages.

CRediT authorship contribution statement

Maria Luisa Celesti: Writing – review & editing, Writing – original draft, Visualization, Validation, Software, Methodology, Investigation, Formal analysis, Data curation, Conceptualization. **Guglielmo Papini:** Writing – review & editing, Validation, Methodology, Investigation. **Edoardo Pasta:** Writing – review & editing, Validation, Methodology, Investigation. **Yerai Peña-Sanchez:** Writing – review & editing, Visualization, Supervision, Methodology, Investigation. **Facundo D. Mosquera:** Writing – review & editing, Visualization, Methodology, Investigation. **Francesco Ferri:** Writing – review & editing, Supervision, Project administration, Methodology, Investigation. **Nicolás Faedo:** Writing – review & editing, Writing – original draft, Visualization, Validation, Supervision, Software, Resources, Methodology, Investigation, Funding acquisition, Formal analysis, Data curation, Conceptualization.

Declaration of competing interest

The authors declare that they have no known competing financial interests or personal relationships that could have appeared to influence the work reported in this paper.

Acknowledgment

Project funded by the European Union - NextGenerationEU under the National Recovery and Resilience Plan (NRRP), Mission 04 Component 2 Investment 3.1 | Project Code: IR0000027 - CUP: B33C22000710006 - iENTRANCE@ENL: Infrastructure for Energy TRAnsition aNd Circular Economy @ EuroNanoLab.

Data availability

Data will be made available on request.

References

[1] G. Mork, S. Barstow, A. Kabuth, M.T. Pontes, Assessing the global wave energy potential, in: International Conference on Offshore Mechanics and Arctic Engineering, Vol. 49118, 2010, pp. 447–454.
[2] J. Cruz, Ocean Wave Energy: Current Status and Future Prespectives, Springer Science & Business Media, 2007.
[3] A.F.d.O. Falcao, Wave energy utilization: A review of the technologies, Renew. Sustain. Energy Rev. 14 (3) (2010) 899–918.
[4] J.V. Ringwood, S. Zhan, N. Faedo, Empowering wave energy with control technology: Possibilities and pitfalls, Annu. Rev. Control (2023).
[5] C. Windt, N. Faedo, M. Penalba, F. Dias, J.V. Ringwood, Reactive control of wave energy devices–the modelling paradox, Appl. Ocean Res. 109 (2021) 102574.
[6] M. Penalba Retes, A. Mérigaud, J.-C. Gilloteaux, J. Ringwood, Nonlinear Froude-Krylov force modelling for two heaving wave energy point absorbers, in: Proceedings of the 11th European Wave and Tidal Energy Conference, 2015.
[7] N. Faedo, G. Giorgi, J. Ringwood, G. Mattiazzo, Optimal control of wave energy systems considering nonlinear Froude–Krylov effects: control-oriented modelling and moment-based control, Nonlinear Dynam. 109 (3) (2022) 1777–1804.
[8] N. Faedo, M.L. Celesti, On the role of modelling uncertainty in optimal control and performance assessment of wave energy conversion systems, in: 34th International Ocean and Polar Engineering Conference, ISOPE 2024, ISOPE, 2024, pp. 1–10.
[9] M. Farajvand, V. Grazioso, D. García-Violini, J.V. Ringwood, Uncertainty estimation in wave energy systems with applications in robust energy maximising control, Renew. Energy 203 (2023) 194–204.
[10] M. Farajvand, D. García-Violini, J.V. Ringwood, Representative linearised models for a wave energy converter using various levels of force excitation, Ocean Eng. 270 (2023) 113635.
[11] M.L. Celesti, F. Ferri, N. Faedo, Experimental modelling uncertainty quantification for a prototype wave energy converter, in: European Control Conference, ECC, 2024, pp. 1539–1544.
[12] R.H. Hansen, M.M. Kramer, Modelling and control of the wavestar prototype, in: 9th European Wave and Tidal Energy Conference, EWTEC, Southampton, 2011, pp. 1–10.
[13] J. Ringwood, F. Ferri, N. Tom, K. Ruehl, N. Faedo, G. Bacelli, Y.-H. Yu, R.G. Coe, The wave energy converter control competition: Overview, in: International Conference on Offshore Mechanics and Arctic Engineering, Vol. 58899, 2019, V010T09A035.
[14] C. Windt, N. Faedo, D. García-Violini, Y. Peña-Sanchez, J. Davidson, F. Ferri, J.V. Ringwood, Validation of a CFD-based numerical wave tank model of the 1/20th scale wavestar wave energy converter, Fluids 5 (3) (2020) 112.
[15] S. Heo, W. Koo, Dynamic response analysis of a wavestar-type wave energy converter using augmented formulation in Korean nearshore areas, Processes 9 (10) (2021) 1721.
[16] N. Tom, K. Ruehl, F. Ferri, Numerical model development and validation for the WECCCOMP control competition, in: International Conference on Offshore Mechanics and Arctic Engineering, Vol. 51319, American Society of Mechanical Engineers, 2018, V010T09A042.
[17] N. Faedo, Y. Peña-Sanchez, E. Pasta, G. Papini, F.D. Mosquera, F. Ferri, SWELL: An open-access experimental dataset for arrays of wave energy conversion systems, Renew. Energy 212 (2023) 699–716.
[18] M. Penalba, G. Giorgi, J.V. Ringwood, Mathematical modelling of wave energy converters: A review of nonlinear approaches, Renew. Sustain. Energy Rev. 78 (2017) 1188–1207.
[19] J. Falnes, A. Kurniawan, Ocean Waves and Oscillating Systems: Linear Interactions Including Wave-Energy Extraction, vol. 8, Cambridge University Press, 2020.
[20] J. Davidson, R. Costello, Efficient nonlinear hydrodynamic models for wave energy converter design—A scoping study, J. Mar. Sci. Eng. 8 (1) (2020) 35.
[21] E. Pasta, N. Faedo, G. Mattiazzo, J.V. Ringwood, Towards data-driven and data-based control of wave energy systems: Classification, overview, and critical assessment, Renew. Sustain. Energy Rev. 188 (2023) 113877.
[22] M.P. Schoen, J. Hals, T. Moan, Wave prediction and robust control of heaving wave energy devices for irregular waves, IEEE Trans. Energy Convers. 26 (2) (2011) 627–638.
[23] G. Bacelli, R.G. Coe, D. Patterson, D. Wilson, System identification of a heaving point absorber: Design of experiment and device modeling, Energies 10 (4) (2017) 472.
[24] N. Faedo, E. Pasta, F. Carapellese, V. Orlando, D. Pizzirusso, D. Basile, S.A. Sirigu, Energy-maximising experimental control synthesis via impedance-matching for a multi degree-of-freedom wave energy converter, IFAC-PapersOnLine 55 (31) (2022) 345–350.
[25] E. Pasta, G. Papini, Y. Peña-Sanchez, F.D. Mosquera, F. Ferri, N. Faedo, Data-based modelling of arrays of wave energy systems: Experimental tests, models, and validation, Control Eng. Pract. 148 (2024) 105949.
[26] E. Pasta, G. Papini, Y. Peña-Sanchez, F.D. Mosquera, F. Ferri, N. Faedo, OCEAN-open-access validated models from experimental data of wave energy system arrays, 2024, http://dx.doi.org/10.17632/97cpczdg2r.1.
[27] L. Ljung, System identification, in: Signal Analysis and Prediction, Springer, 1998, pp. 163–173.
[28] R. Pintelon, J. Schoukens, System Identification: A Frequency Domain Approach, John Wiley & Sons, 2012.
[29] M.S. Bartlett, Smoothing periodograms from time-series with continuous spectra, Nature 161 (4096) (1948) 686–687.
[30] J. Falnes, On non-causal impulse response functions related to propagating water waves, Appl. Ocean Res. 17 (6) (1995) 379–389.
[31] T. McKelvey, H. Akçay, L. Ljung, Subspace-based multivariable system identification from frequency response data, IEEE Trans. Autom. Control 41 (7) (1996) 960–979.
[32] A. Babarit, G. Delhommeau, Theoretical and numerical aspects of the open source BEM solver NEMOH, in: 11th European Wave and Tidal Energy Conference, EWTEC2015, 2015.
[33] D.E. Hasselmann, M. Dunckel, J. Ewing, Directional wave spectra observed during JONSWAP 1973, J. Phys. Oceanogr. 10 (8) (1980) 1264–1280.
[34] N. Faedo, F.J. Dores Piuma, G. Giorgi, J.V. Ringwood, Nonlinear model reduction for wave energy systems: a moment-matching-based approach, Nonlinear Dynam. 102 (3) (2020) 1215–1237.
[35] N. Faedo, F.D. Mosquera, E. Pasta, G. Papini, Y. Peña-Sanchez, C.A. Evangelista, F. Ferri, J.V. Ringwood, P. Puleston, Experimental assessment of combined sliding mode & moment-based control (SM2C) for arrays of wave energy conversion systems, Control Eng. Pract. 144 (2024) 105818.
[36] N. Faedo, D. García-Violini, G. Scarciotti, A. Astolfi, J.V. Ringwood, Robust moment-based energy-maximising optimal control of wave energy converters, in: 58th Conference on Decision and Control, CDC, 2019, pp. 4286–4291.